Bull. Soc. Chim. Belg. vol.92/n°10/1983

ROVIBRONIC STRUCTURE AND THE DYNAMICS OF THE PREDISSOCIATION PROCESSES $HNO(A\ ^1A'') \rightarrow H(^2S) + NO(X^2\Pi)$ AND $HONO(\tilde{A}\ ^1A'') \rightarrow OH(X^2\Pi) + NO(X^2\Pi)$

R.N. DIXON
School of Chemistry, The University, Bristol BS8 1TS, U.K.

Invited lecture given at the XVIth International Symposium on Free Radicals
September 12-16,1983, Lauzelle-Ottignies,Belgium

INTRODUCTION

The dynamics and mechanism of the predissociation of a polyatomic molecule may be studied experimentally either (i) through measurement of line-broadening of lifetimes of excited levels of the parent, or (ii) through probing the nascent photofragments following well characterised parent molecule excitation. Spectroscopic perturbations in the parent may be brought about by the same coupling operator as mixes the bound and unbound levels, so that structure and dynamics are inter-related. In this paper we compare the experimental data and deduced predissociation mechanisms of *HNO and HONO*, both of which have low-lying $\tilde{A}\ ^1A''$ excited states of the π^*-n type within the -N=O chromophore. In the first of these the measurements are entirely those of the properties of the parent molecule; whereas in the second the nascent OH has been characterised in considerable detail.

$HNO(\tilde{A}\ ^1A'') \rightarrow H(^2S) + NO(X^2\Pi)$

Ten absorption bands of the $\tilde{A}\ ^1A'' - \tilde{X}\ ^1A'$ electronic transition HNO, and nine of *DNO*, were discovered in the red and near infra-red by Dalby (1) and by later workers (2) using flash photolysis. All three upper state vibrations are Franck-Condon active to at least one quantum. A number of rotational perturbations were noted. Line-broadening of up to 0.7 cm^{-1} was observed in the 101 level of HNO, equivalent to a predissociation lifetime of ≥8 ps. (2,3). Medium resolution emission spectra of HNO and DNO showed a sharp breaking off in the K-rotational structure, giving upper limits to the dissociation energies (4), although these limits have since been revised downwards.

Recent experiments using laser-induced fluorescence excitation (LIF) have greatly increased the resolution, sensitivity and variety of spectroscopic studies on HNO and DNO (5-8). The radiative lifetime of the $\tilde{A}$ state is ca 23μs (7), so that breaking off in emission can result from a predissociation rate as low as 10^6 s^{-1}. In a recent study we have observed fluorescence of HNO from the J=0 levels of the 101 and 030 vibronic state lying above the dissociation limit; and have observed in other vibronic states that the breaking-off energy is a function of J', but not of K' or the vibrational quantum numbers (6). Analytical potentials for the $\tilde{A}$, $\tilde{X}$ and $\tilde{a}\ ^3A''$ states were derived using all available data, thereby showing that at threshold the predissociation occurs through Coriolis coupling of the levels of the $\tilde{A}$ state to high levels of the ground state (6). Direct dissociation at this energy is prevented by a 2300 cm^{-1} barrier between the $\tilde{A}$ state potential well and the H+NO asymptote.

These LIF measurements have now been much extended on both HNO and DNO, resulting in more complete band analyses (9). Numerous rotational perturbations have been found. Some of these are accompanied by strong magnetic sensitivity, and in one case (the K'=5, J'=8 level of the HNO 000 state) a complete Paschen-Back effect is observed which can only be interpreted as interaction with levels of the $\tilde{a}\ ^3A''$ state. Even so the greater number are non-magnetic, and appear to be singlet-singlet (Coriolis) interactions.

These new measurements include detection of the 002 and 003 vibronic states of HNO (Figure 1), so that all the vibronic levels of the $\tilde{A}$ state below the dissociation limit are now known. The bending vibration is remarkably harmonic (successive intervals are 981, 979 and 975 cm^{-1}). This trend is strongly at variance with predictions from our earlier potential function (6), with an error of ~300 cm^{-1} for the 003 term value. Furthermore, the fit to all the vibronic data of HNO and DNO cannot be greatly improved by refining the potential within the constraints of the model used. These large errors arise from the neglect of Renner-Teller coupling between the $\tilde{A}$ and $\tilde{X}$ states.

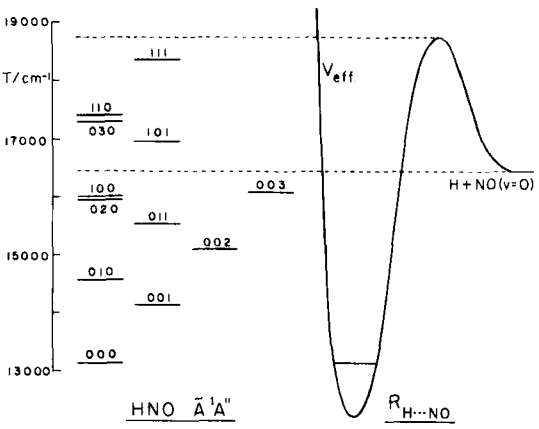

FIG. 1. The relationship between the known $\tilde{A}$ state vibronic levels of HNO and the effective potential along the dissociation coordinate.

Both on molecular orbital arguments, and by correlation with the states of O_2, it is known that for bond lengths close to equilibrium the $\tilde{A}$ and $\tilde{X}$ states correlate with a $^1\Delta$ state of linear HNO. Consequently the total wave-function must in general include a linear combination of two products of electronic and nuclear functions (10,11) :

$$\psi = \psi_e^{+}(r_e,r_n)\chi^{+}(r_n) + \psi_e^{-}(r_e,r_n)\chi^{-}(r_n) \qquad (1)$$

where ψ_e^{+} transforms as $^1A'$ and ψ_e^{-} as $^1A''$. The effective potential for the vibronic origins of the $\tilde{A}\ ^1A''$ state, for which $K_a'=0$, is obtained by adding $A(r_n)\Lambda^2 = 4A(r_n)$ to its Born-Oppenheimer potential. The rotational 'constant' $A(r_n)$ becomes infinite for linear HNO. As a result of this the marked anharmonicity associated with the convergence of the bending levels of a quasi-linear non-degenerate state is much less apparent for a component of a Δ state (12). A new potential function for HNO and DNO has been generated incorporating this orbital contribution; and we are now all to fit all the available vibronic states to 10 cm^{-1} or better, thus proving the necessity to take account of the orbital angular momentum (13).

Within the above model the importance to the $\tilde{A}$ state levels of $\chi^+(r_n)$ relative to $\chi^-(r_n)$ depends on the matrix elements of the Coriolis operator $-2A(r_n)J_aL_a - 2B(r_n)J_bL_b$, and therefore increases with increase in K_a and to a lesser degree J. To the extent that the bending motion is approximately separable from the stretching motions this mixing should also increase with increasing ν_3. This accords with the observation of a K-dependent line broadening in the 101 vibronic state of HNO, whereas no broadening outside the Doppler limit was observed in the higher energy 030 and 110 states. Furthermore, the bound 002 and 003 states exhibit extensive rotational perturbations.

Finally, we have observed breaking-off of the J-structures of DNO LIF excitation bands, and fitted these to the same threshold model as for HNO, yielding $D_0^o(DNO) = 17030 \pm 10\ cm^{-1}$, compared with $D_0^o(HNO) = 16450 \pm 10\ cm^{-1}$. The difference in total ground state zero point energy of HNO and DNO, computed from our potential function, is 3004-2440 = 564 cm^{-1}. This agrees closely with the difference in dissociation energies, and confirms the proposed dissociation mechanism.

HONO($\tilde{A}\ ^1A''$) → OH($X^2\Pi$) + NO($X^2\Pi$)

The origin of the near u.v. band system of trans HONO (ν_{00}=26034 cm^{-1}) (14) lies 9160 cm^{-1} above the dissociation limit to ground state OH and NO, and the whole system is predissociated. The principal progression is in the terminal -N=O stretching vibration $\nu_2' \sim 1140\ cm^{-1}$. All the bands have a width of ~50 cm^{-1}, corresponding to a predissociation lifetime of 0.1 ps which is much faster than molecular rotation (although part of this width may be due to incipient rotational structure). The near unity quantum yield to give OH+NO (15) make HONO a very attractive candidate for using pulsed excitation lasers in a detailed study of the nascent photofragments. In particular, the transient nature of the OH radical permits its detection without interference from any background concentration.

Most of the past photodissociation experiments have involved the measurement of only one of either (a) fragment vectorial properties such as angular distributions through mass spectrometry and recoil velocities through time-of-flight mass analysis; or (b) scalar properties such as the internal state population distribution using dispersed fluorescence for excited products or LIF for ground state products. In a preliminary study we have shown that by combining Doppler and polarization spectroscopy with LIF it is possible to simultaneously measure all the desired scalar and vectorial properties (16). The OH fragment has now been probed in such detail following excitation of trans HONO in the 2_0^1, 2_0^2 and 2_0^3 bands (17).

Figure 2 compares the excitation spectrum of photofragment OH with that of 300K thermalised OH, generated using the $H+NO_2 \rightarrow OH+NO$ reaction with collisional equilibration. The photofragment OH is rotationally and vibrationally cold, but the internal state population distribution shows a marked departure from statistical equilibrium. The relative intensities of high J lines are also sensitive to the polarisation geometry of the photolysis and probe electric vectors, indicating that the rotational distribution is anisotropic. From these observations we may conclude that (i) the $F_1(J=N+\frac{1}{2})$ and $F_2(J=N-\frac{1}{2})$ fine structure components are not in equilibrium with each other, although the mem-

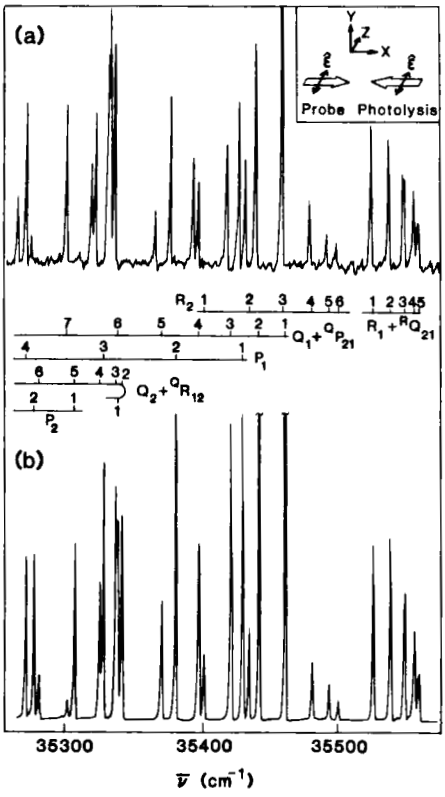

FIG. 2. Comparison of the excitation spectra of the A $^2\Sigma^+$ - X$^2\Pi$(1,0) band of (a) OH from photolysis of HONO at 369 nm, and (b) thermalised OH. The inset gives the pump/probe geometry. The photomultiplier is along the Z axis, and detects all polarisations.

bers of each of these are reasonably well characterised by "temperatures" of about 360K for the F_1 levels and 250K for the F_2 levels. The F_2/F_1 population ratios are N-dependent, and vary with photolysis wavelength. For N=1 the ratios are 1.81 for 369 nm (2^1_0), 1.66 for 355 nm (2^2_0) and 1.33 for 342 nm (2^3_0), whereas this ratio is less than one for thermal equilibrium. (ii) The $^2\Pi^+$(N)/$^2\Pi^-$(N) Λ-doublet population ratio is anomalously large by a factor which increases with N, and is about 2.3 for N=5. (iii) The fragment rotation is preferentially aligned parallel to the photolysis electric vector, and hence parallel to the HONO transition moment, especially at high N.

High resolution spectra show that the OH lines are all anomalously broad and double-peaked (Figure 3). This line profile arises from a large and highly anisotropic fragment recoil. It can be quantitatively simulated using an OH translational energy of 4490 cm^{-1}, and an asymmetry parameter

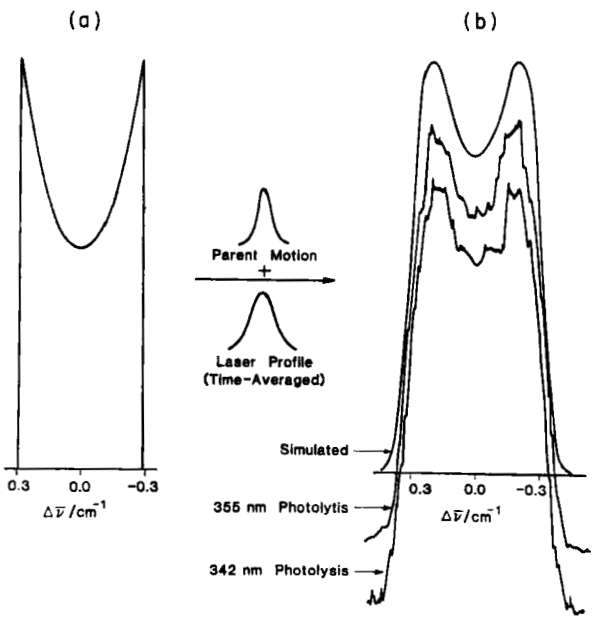

FIG. 3. The computed OH Doppler-split line shape (a) calculated in the centre of mass frame for a single Doppler shift of 0.295 cm^{-1} and an anisotropy parameter β= -0.8, and (b) after convoluting (a) with the HONO thermal motion and the measured laser line profile. This is compared with the experimental profiles of the P_1(1) line shape for the OH photofragment generated by 355 nm and 342 nm photolysis.

$\beta = -0.8$, indicating a strong propensity for recoil perpendicular to the HONO transition moment. Surprisingly this profile is not only independent of the OH rotational state, but also of the photolysis wavelength. Thus energy does not flow from the excited terminal -N=O vibration to the HO-NO dissociation coordinate over the timescale of the fragmentation.

The analysis of these observations leads to the following conclusions concerning the dissociation dynamics : (i) the HONO transition moment is perpendicular to the HONO plane, as previously suspected, and dissociation takes place largely within this plane on a timescale fast compared with its rotation. (ii) The spins of the odd electrons on the nascent OH and NO fragments remain coupled to give a singlet while the central bond is cleaved, so that spin and nuclear rotation evolve independently. (iii) The orbital of the unpaired OH electron originates in the HONO plane. (iv) At high N the OH rotation derives predominantly from the zero point vibrational momentum of the in-plane HON bending vibration ν_3. Lower fragment rotation originates both from ν_3 and the out-of-plane torsional vibration ν_6, and is thus more isotropic. (v) The energy available to the OH fragment due to the impulse associated with the O-N bond cleavage is channelled mostly into translation.

Is the HONO $\tilde{A}$ state short-lived because of predissociation by another electronic state, or because the diabatic $\tilde{A}$ state surface is itself not bound along the dissociation coordinate S_4? A recent ab-initio calculation shows that the $\tilde{A}$ state correlates smoothly with ground state products (18), but does not present a complete surface. The relative sharpness of the HONO vibronic structure indicates that the $\tilde{A}$ state surface cannot be strongly repulsive along the S_4 coordinate in the Franck-Condon region. This points either to an electronic predissociation, or to a vibrational predissociation of Herzberg's type II (19).

Predissociation by the ground state is possible through the mechanism of vibronic interaction involving the out-of-plane torsional vibration ν_6. Since ν_6 is not excited in the upper state this requires the mixing of the 2^n upper state levels with ground state levels having an odd number of quanta of $\nu_6'' = 544\ cm^{-1}$. Half the vibronic levels of the $\tilde{X}$ state satisfy this symmetry requirement. As with HNO the $\tilde{A}$ and $\tilde{X}$ states will become the components of a $^1\Delta$ state for linear HONO. Thus we may envisage the nuclear kinetic energy operator playing the same coupling role between the $\tilde{A}$ and $\tilde{X}$ states of HONO as does the Coriolis operator in HNO, leading to predissociation after a few periods of the torsional vibration.

The alternative vibrational mechanism requires an $\tilde{A}$ state surface that is relatively flat along S_4 in the Franck-Condon region, giving a lifetime long enough for the ν_2' vibration to be well developed, but becomes increasingly repulsive as S_4 (the central HO-NO bond) is stretched. Pack has proposed similar surfaces to be responsible for the structured nature of many diffuse polyatomic absorption spectra (20), although his examples involve symmetrical saddle points.

Either of these two mechanisms is capable of accommodating all the present observations. Further experimental and theoretical work will be needed before a decision can be made between them.

CONCLUSION

This paper attempts to present a unifying framework for understanding the dissociation dynamics of HNO and of HONO. It should also find application to the photodissociation of other nitroso compounds, several of which are currently being studied in a number of laboratories.

I am indebted to my collaborators S. Carter, K.B. Jones, M. Noble, K.R. Rosser, C.A. (Taylor) Rosser, R. Vasudev and R.N. Zare without whom this paper could not have been written. I am also grateful to the British S.E.R.C. and to N.A.T.O. for financial support.

REFERENCES

1. F.W. Dalby, Can. J. Phys. 36, 1336 (1958).
2. J.L. Bancroft, J.M. Hollas, D.A. Ramsay, Can. J. Phys. 40, 322 (1962)
3. P.A. Freedman, Chem. Phys. Lett. 44, 605 (1976).
4. M.J.Y. Clement, D.A. Ramsay, Can. J. Phys. 39, 205 (1961).
5. R.N. Dixon, M. Noble, Chem. Phys. 50, 331 (1980).
6. R.N. Dixon, K.B. Jones, M. Noble, S. Carter, Mol. Phys. 42, 455 (1981).
7. R.N. Dixon, M. Noble, C.A. Taylor, M. Delhoume, Farad. Disc. Roy. Soc. Chem. 71, 125 (1981).
8. T. Ishiwata, I. Tanaka, H. Akimoto, J. Phys. Chem. 82, 1336 (1978).
9. C.A. Rosser, Ph.D. Thesis, University of Bristol (1983).
10. R. Renner, Z. Phys. 92, 172 (1934).
11. G. Duxbury, R.N. Dixon, Mol. Phys. 43, 255 (1981).
12. R.N. Dixon, Trans. Farad. Soc. 60, 1363 (1964).
13. S. Carter, R.N. Dixon, C.A. Taylor, to be published.
14. G.W. King, D. Moule, Can. J. Chem. 40, 2057 (1962).
15. R.A. Cox, R.G. Derwent, J. Photochem. 6, 23 (1976/7).
16. R. Vasudev, R.N. Zare, R.N. Dixon, Chem. Phys. Lett. 96, 399 (1983).
17. R. Vasudev, R.N. Zare, R.N. Dixon, to be published.
18. C. Larrieu, A. Dargelos, M. Chaillet, Chem. Phys. Lett. 91, 465 (1982).
19. G. Herzberg, Electronic Spectra of Polyatomic Molecules, Van Nostrand, N.Y. (1966).
20. R.T. Pack, J. Chem. Phys. 65, 4765 (1976).